The Astrophysical Journal, 972:114 (9pp), 2024 September 1 https://doi.org/10.3847/1538-4357/ad5a12

Origin of the Strong Sodium Absorption of the Lensed Supernova 2016geu at $z = 0.4$

Christa Gall[1], Jens Hjorth[1], Lise Christensen[2], Luca Izzo[1,3], Paolo A. Mazzali[4,5], Mark M. Phillips[6], Peter Hoeflich[7], Charlotte Angus[1,8], Cecilie Cold[1], and Jonatan Selsing[1]
[1] DARK, Niels Bohr Institute, University of Copenhagen, Jagtvej 155A, DK-2200 Copenhagen N, Denmark; christa.gall@nbi.ku.dk
[2] Cosmic Dawn Center, Niels Bohr Institute, University of Copenhagen, Jagtvej 155A, DK-2200 Copenhagen N, Denmark
[3] INAF, Osservatorio Astronomico di Capodimonte, Salita Moiariello 16, I-80131 Napoli, Italy
[4] Astrophysics Research Institute, Liverpool John Moores University, ic2, 146 Brownlow Hill, Liverpool L3 5RF, UK
[5] Max-Planck Institut für Astrophysik, Karl-Schwarzschild-Str. 1, 85741, Garching, Germany
[6] Carnegie Observatories, Las Campanas Observatory, Casilla 601, La Serena, Chile
[7] Florida State University, Tallahassee, FL, USA
[8] Astrophysics Research Centre, School of Mathematics and Physics, Queen's University Belfast, Belfast BT7 1NN, UK
Received 2024 May 8; revised 2024 June 15; accepted 2024 June 16; published 2024 August 28

Abstract

The origin of strong sodium absorption, which has been observed for a few nearby Type Ia supernovae (SNe Ia), remains elusive. Here we analyze two high-signal-to-noise, intermediate-resolution Very Large Telescope/X-shooter spectra at epochs +18 and +27 days past peak brightness of the strongly lensed and multiply imaged Type Ia SN 2016geu, which exploded at a redshift of $z = 0.4$. We show that SN 2016geu exhibits very strong multiple Na I and Ca II absorption lines with a large total Na I D rest-frame equivalent width (EW) of 5.2 ± 0.2 Å, among the highest ever detected for an SN Ia and similar to only a handful of nearby SNe Ia with extraordinarily large Na I D EWs. The absorption system is time-invariant and extends over a large velocity span ~250 km s^{-1}. The majority of the absorption is blueshifted relative to the strongest component, while there are both blueshifted and redshifted components relative to the systemic redshift of the galaxy. The column density ratios and widths of the absorption lines indicate that the absorption likely arises from a combination of interstellar dusty molecular clouds and circumgalactic in- and outflowing material rather than circumstellar matter around the supernova.

Unified Astronomy Thesaurus concepts: Type Ia supernovae (1728); Interstellar absorption (831); Circumstellar matter (241)

1. Introduction

Type Ia supernovae (SNe Ia) are among the most powerful explosions in the Universe. Their progenitors consist of a close binary stellar system in which a carbon–oxygen degenerate white dwarf undergoes a thermonuclear runaway (e.g., Hoyle & Fowler 1960; Hillebrandt & Niemeyer 2000; Höflich et al. 2011). While the classical scenarios include the double-degenerate (Iben & Tutukov 1984; Webbink 1984) model and the single-degenerate model (Whelan & Iben 1973; Nomoto 1982), a wide variety of progenitor systems and mechanisms triggering the terminal explosion have been proposed (for a review see Livio & Mazzali 2018 and references therein).

Complex Na I D absorption systems with multiple components have been observed in several SNe Ia in the nearby Universe (D'Odorico et al. 1989; Blondin et al. 2009; Simon et al. 2009; Sternberg et al. 2011; Foley et al. 2012; Maguire et al. 2013; Phillips et al. 2013; Ritchey et al. 2015). Blueshifted components have traditionally been attributed to circumstellar material that has been ejected during the presupernova phase (Sternberg et al. 2011; Maguire et al. 2013; Phillips et al. 2013; Clark et al. 2021). In some of these SNe Ia with blueshifted Na I D components, e.g., SN 2006X (Patat et al. 2007), SN 2007le (Simon et al. 2009), or iPTF11kx (Dilday et al. 2012), the absorption strength, or equivalent width (EW), was found to vary over several days around peak brightness of the supernova. The time variability has been explained as an effect of ionization and subsequent recombination of Na I D in shells or clumps of outflowing circumstellar material (Patat et al. 2007). The latter is the relic of presupernova evolution (Patat et al. 2007, 2011; Dilday et al. 2012; Raskin & Kasen 2013; Soker et al. 2013). In other systems, e.g., SN 1986G (D'Odorico et al. 1989) and SN 2014C (Ritchey et al. 2015), strong Na I D absorption has been attributed to interstellar material.

Aided by strong magnification due to gravitational lensing, the multiply imaged SN 2016geu at $z = 0.4$ can shed new light on the origin of strong Na I D absorption. SN 2016geu was discovered by the intermediate Palomar Transient Factory on 2016 September 5 in the Sloan Digital Sky Survey galaxy J210415.89-062024.7 and was classified as a normal SN Ia (Goobar et al. 2017; Cano et al. 2018; Johansson et al. 2021). A thorough spectroscopic analysis (Cano et al. 2018) revealed that SN 2016geu belongs to groups of both high-velocity and high-velocity-gradient (Benetti et al. 2005) and core-normal SNe Ia (Branch et al. 2006). It appeared ~70 times brighter than an unlensed SNe Ia at the same redshift due to gravitational lensing (and possibly microlensing) magnification (Goobar et al. 2017; More et al. 2017; Dhawan et al. 2020). We obtained two optical to near-infrared medium-resolution Very Large Telescope (VLT)/X-shooter spectra (Cano et al. 2018; Johansson et al. 2021) past peak brightness. The large magnification led to an unprecedented signal-to-noise ratio of the medium-resolution spectra of a $z = 0.4$ supernova.

Here we present a detailed analysis of the Na I D and Ca H and K absorption line complex of SN 2016geu. The Na I D complex was previously studied by Johansson et al. (2021). The paper is organized as follows: the data and the analysis of the Na I D and Ca H and K absorption complex are described

in Section 2 and Section 3, respectively. Other absorption and emission lines are analyzed and discussed in the Appendix. We discuss the origin of the individual Na I D and Ca H and K absorption components in Section 4 and conclude in Section 5.

2. Data

The optical to near-infrared medium-resolution spectra of SN 2016geu (Cano et al. 2018) were obtained with the X-shooter echelle spectrograph (D'Odorico et al. 2006; Vernet et al. 2011) mounted at the Cassegrain focus of the Kueyen unit of the VLT at the European Southern Observatory (ESO) on Cerro Paranal, Chile. They were obtained at two epochs, 2016 October 18.02 UT (57679.02 Modified Julian Date (MJD)) and 2016 October 30.03 UT (57691.03 MJD), which correspond to rest-frame epochs of about +18.6 and +27.1 days past peak brightness (Goobar et al. 2017; Dhawan et al. 2020), respectively. Both observations were performed at a position angle of 86° following the convention "North up–East left," with "ABBA" nodding between exposures along the 11″ slit.

We used the ESO/`ESOReflex` workflow versions 2.9.2 of the X-shooter pipeline (Modigliani et al. 2010; Freudling et al. 2013) to reduce the supernova and the (telluric) standard star spectra to two-dimensional, bias-subtracted, flat-field-corrected, order-rectified, and wavelength- and flux-calibrated spectra. All wavelengths were calibrated in the vacuum frame. Throughout, line transitions are discussed in the astrophysical common notation of air wavelength, with conversions between the two systems performed as given in Morton (1991). To obtain one-dimensional spectra, the two-dimensional spectra from the pipeline were optimally extracted using the full extraction profile for the spectral trace (Horne 1986). Furthermore, the spectra were slit-loss corrected and corrected for heliocentric velocities. Telluric corrections were applied using molecfit (Kausch et al. 2015; Smette et al. 2015). All calibrations and correction procedures were performed after the basic pipeline reduction using refined custom `python` programs (Selsing et al. 2019). The spectra were corrected for a Galacticextinction along the line of sight to the supernova of $E(B-V)$ of 0.31 ± 0.05 mag for $R_V = 3.1$ (Schlafly & Finkbeiner 2011). The spectra were lens-galaxy subtracted using the lens model of Goobar et al. (2017) as described in Cano et al. (2018).

3. The Sodium and Calcium Absorption Line Complex

SN 2016geu exhibits prominent sodium and calcium absorption line complexes. The sodium doublet, Na I D, corresponds to the fine structure splitting of the neutral sodium excited states observed in air at $\lambda\lambda$5889.95 (D_2) and 5895.92 (D_1) Å respectively. The calcium doublet, Ca II H and K, corresponds to the fine structure splitting of the singly ionized calcium excited states observed in air at $\lambda\lambda$3968.46 (K) and 3933.65 (H) Å. We use a redshift of $z = 0.408788$ (Na I D component B) as the systemic redshift of the host galaxy and the reference redshift for all components.

3.1. Analysis of the Absorption Line Components

We identify and estimate the column densities of Na I D and Ca II H and K components using the `python` package `VoigtFit` (Krogager 2018). The continuum normalization is done interactively using second- and fifth-order Chebyshev polynomials for Na I D and Ca II H and K, respectively. Higher-order polynomials are required since the absorption lines are on top of stronger, high-velocity absorption features from SN Ia ejecta elements. As per the definition of `VoigtFit`, the main parameters, e.g., the ratio of a transition's oscillator strengths, f-values, are fixed such that the relative velocity, Doppler broadening parameter, b, and column density for different transitions of the same ionization state are identical. This means that the fitted parameters such as the b-values, column densities, and the relative velocities of Na I D_1 and Ca II H will be the same as those of Na I D_2 and Ca II K.

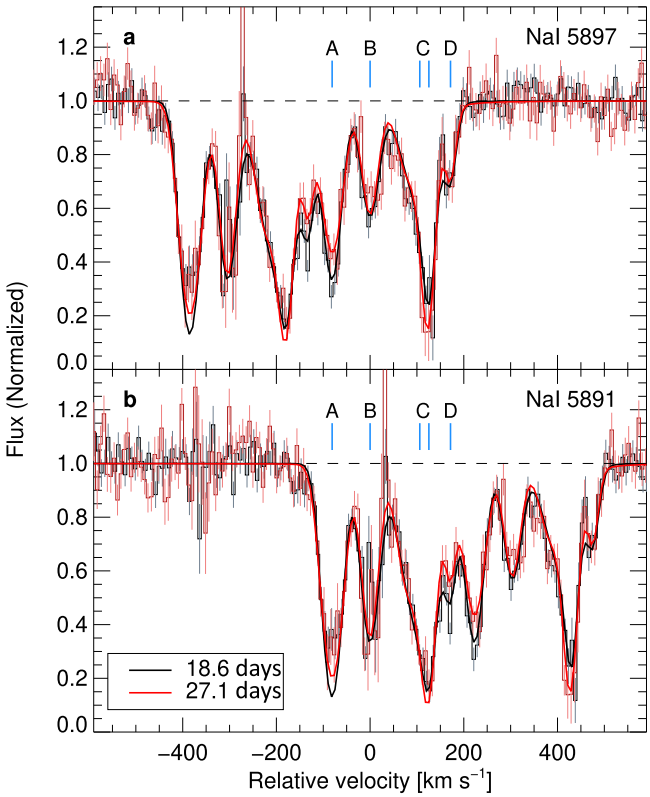

Figure 1. The sodium absorption line complex of SN 2016geu. The panels show (a), Na I D_1 λ5897, and (b), Na I D_2 λ5891. The data are shown as thin black and red lines including errors on the data for rest-frame epochs at +18.6 and +27.1 days, respectively. The black and red solid lines are Voigt profile fits (Section 3) at the respective epochs. Five velocity components are identified and labeled as A, B, C, and D, of which component C consists of two subcomponents C1 and C2. The horizontal dashed line indicates 1.0 in normalized flux units. All velocities are given relative to the redshift of component B, $z = 0.408788$.

The EW and full width at half-maximum (FWHM) of individual components of Na I D and Ca II H and K are derived from the Voigt profile fits to the absorption lines. The EWs are calculated as $W_\lambda = \int_{\lambda_2}^{\lambda_1} (1 - \frac{F_\lambda}{F_C})\, d_\lambda$, with F_λ and F_C being the observed flux of the line and the continuum flux within the wavelength interval [λ_1, λ_2], respectively. The FWHM of the Voigt profiles is estimated as the full width at half the peak intensity of the line. For other ions the FWHM and minimum absorption velocities are derived from either Gaussian or Lorentzian profile fits to the absorption lines. All measured quantities of absorption lines, including those of Na I D and Ca II H and K of the lens galaxy, are summarized in Tables 1 and 2.

Table 1
Measured Properties of Individual Absorption Lines

Component	Ion	Redshift[a]	EW[b] (Å)	D_2/D_1 K/H	FWHM (km s^{-1})	log(N) (cm^{-2})	b (km s^{-1})	v_{rel}[c] (km s^{-1})
			MJD 57679.0075					
A	Na I D_1	0.408407(3)	0.65(12)	1.34(31)	47.3(1.4)	13.02(0.03)	19.98(1.08)	−81.0(0.6)
	Na I D_2		0.88(12)		52.6(1.3)			
B	Na I D_1	0.408788(6)	0.40(12)	1.62(60)	45.4(2.6)	12.71(0.03)	19.95(2.04)	0.0(0.0)
	Na I D_2		0.65(12)		48.0(2.6)			
C1	Na I D_1	0.409287(86)	0.62(13)	1.7(43)	84.3(36.6)	12.89(0.30)	44.44(11.27)	106.1(18.3)
	Na I D_2		1.07(15)		89.8(36.6)			
C2	Na I D_1	0.409378(15)	0.44(13)	1.2(48)	31.1(6.5)	15.68(1.93)	3.04(2.6)	125.6(3.2)
	Na I D_2		0.56(13)		33.8(6.3)			
D	Na I D_1	0.409595(17)	0.17(12)	1.5(132)	30.9(7.4)	12.31(0.20)	8.67(8.25)	171.7(3.6)
	Na I D_2		0.25(13)		31.3(7.5)			
Lens	Na I D_1	0.21628(22)	0.82(11)	1.6(26)	57.8(5.4)	12.91(0.04)	96.10(4.25)	2.47(2.47)
	Na I D_2		1.36(11)		59.9(5.5)			
A	Ca II H	0.408412(15)	0.34(12)	1.74(71)	79.25(6.4)	12.94(0.05)	39.35(5.92)	−80.0(3.2)
	Ca II K		0.59(12)		83.23(6.4)			
C1	Ca II H	0.409299(46)	0.42(12)	1.6(54)	74.89(19.6)	13.07(0.12)	35.49(10.60)	108.8(9.8)
	Ca II K		0.67(12)		79.65(19.6)			
D	Ca II H	0.409582(72)	0.14(12)	2.0(195)	54.15(30.6)	12.58(0.33)	22.17(16.71)	169.1(15.3)
	Ca II K		0.28(13)		54.71(30.6)			
Lens	Ca II H and K	0.2162(112)	11.62(29)	…	…	…	…	…
			MJD 57691.0131					
A	Na I D_1	0.408409(6)	0.60(12)	1.5(36)	52.3(2.6)	12.93(0.04)	23.8(2.00)	−80.6(1.3)
	Na I D_2		0.92(12)		57.2(2.6)			
B	Na I D_1	0.408787(9)	0.35(12)	1.6(64)	40.1(3.9)	12.66(0.05)	16.83(3.22)	−0.2(0.2)
	Na I D_2		0.57(12)		42.5(3.9)			
C1	Na I D_1	0.40917(46)	0.25(13)	1.8(106)	52.4(19.6)	12.48(0.21)	25.96(11.9)	81.3(9.8)
	Na I D_2		0.46(13)		54.3(19.6)			
C2	Na I D_1	0.409368(11)	0.80(13)	1.2(26)	39.6(4.7)	16.27(0.32)	4.33(1.06)	123.4(2.3)
	Na I D_2		0.98(13)		45.1(4.7)			
D	Na I D_1	0.409593(12)	0.16(13)	1.4(142)	27.9(5.1)	12.43(0.34)	3.95(2.56)	171.3(2.4)
	Na I D_2		0.21(13)		27.8(5.1)			
Lens	Na I D_1	0.21628(28)	0.72(11)	1.7(30)	67.9(8.4)	12.87(0.06)	87.32(10.17)	9.37(4.2)
	Na I D_2		1.22(11)		71.5(8.4)			
A	Ca II H	0.408415(21)	0.41(12)	1.76(60)	79.73(8.9)	13.07(0.07)	38.63(7.61)	−79.2(4.5)
	Ca II K		0.72(12)		84.31(8.9)			
C1	Ca II H	0.409303(33)	0.57(12)	1.74(42)	139.92(14.1)	13.17(0.07)	75.99(11.78)	109.7(7.1)
	Ca II K		0.99(12)		147.63(14.1)			
Lens	Ca II H and K	0.21621(77)	14.92(28)	…	…	…	…	…

Notes. All parameters are obtained using `VoigtFit` (Krogager 2018) and a custom `IDL` program.
[a] Errors are multiplied by 10^6.
[b] EWs are in the rest frame. Errors for the rest-frame EWs are multiplied by 10^2.
[c] All velocities are with respect to either $z = 0.408788$, corresponding to component B of Na I D or $z = 0.2162$ for the lens galaxy.

3.2. The Sodium and Calcium Absorption Line Components

Figure 1 displays the remarkably complex absorption line system of the sodium doublet, Na I D, at both epochs. We identify five distinct components (A, B, C1, C2, and D) for each of the Na I D_1 λ5897 and Na I D_2 λ5891 transitions, spanning a velocity range of about 250 km s^{-1}. The Na I D_1 and D_2 are not fully separated but overlap around component A of Na I D_1 and component D of Na I D_2. Separating Na I D_1 and D_2 results in rest-frame EWs of 2.29 ± 0.28 Å and 3.40 ± 0.29 Å, respectively. The total rest-frame EW of the entire Na I D complex is 5.2 ± 0.2 Å. In an independent analysis, Johansson et al. (2021) found that the sodium complex has three components and reported a total sodium rest-frame EW of 3.9 and 3.3 Å at the two epochs, respectively.

Figure 2 shows a comparison between the Na I D and Ca II H and K absorption complexes. For the Ca II H and K lines we identify three velocity components at similar positions as the Na I D components A, C1, and D. We do not identify a Ca II counterpart to the Na I D component B. The Ca II component C1 is broader than the Na I D C1. This is likely due to it being blended with C2. Due to the lower signal-to-noise ratio at the position of Ca II than around Na I D we cannot unambiguously identify a Ca II component C2. For the second epoch (+27.1 days) the Ca II components C and D are blended. The position of the component C + D remains similar to that of C1.

Table 2
Measured Properties of Absorption Complexes

Ion	EW[a] (Å)	D_2/D_1[a]	EW[a] (Å)	D_2/D_1[a]	log(*N*) (cm^{-2})	log(*N*) (cm^{-2})
Epoch	18.6 days	18.6 days	27.1 days	27.1 days	18.6 days	27.1 days
Na I D	5.2(21)		5.06(26)		15.68(1.93)	16.26(0.58)
Na I D_1[b]	2.29(28)	1.48(22)	2.16(28)	1.44(23)	⋯	⋯
Na I D_2[b]	3.40(29)		3.13(28)			
		K/H		K/H		
Ca II H and K					13.38(0.34)	13.42(0.22)
Ca II H	0.90(22)	1.7(48)	0.98(17)	1.75(35)	⋯	⋯
Ca II K	1.53(22)		1.71(17)			

Notes. All parameters are obtained using `VoigtFit` (Krogager 2018) and a custom `IDL` program.
[a] EWs are in the rest frame. Errors are multiplied by 10^2.
[b] Total EW calculated from the fit.

Through the Voigt profile fits we obtained *b*-values $\gtrapprox 20\,km\,s^{-1}$ for components A, B, and C1 (Table 1). Although the limiting instrumental resolution for the Na I D complex is $\sim 18\,km\,s^{-1}$, this exceeds the maximum theoretically expected *b*-value by thermal broadening ($\approx 6\,km\,s^{-1}$) of the Na I D and Ca II lines. It is also larger than the observed median *b*-value ($\approx 0.7\,km\,s^{-1}$) of Galactic clouds with a temperature of ∼80 K (Welty et al. 1994) and the highest *b*-values obtained from medium- or high-resolution spectra of other SNe Ia (D'Odorico et al. 1989; Ritchey et al. 2015; Ferretti et al. 2016). This strongly suggests that for SN 2016geu, components A, B, and C1 must consist of several systems that are unresolved in our data. Indeed, other SNe Ia, e.g., SN 1986G, SN 2009le, and SN 2014J, have about 9, 8, and 18 resolved components (D'Odorico et al. 1989; Phillips et al. 2013; Ritchey et al. 2015), respectively.

3.3. Lack of Temporal Evolution of the Na I D EW

Figure 3 and Table 1 show that there is no time variability of the measured quantities (e.g., EW, FWHM, column density) for any of the absorption components of either Na I D nor Ca II H and K. On the other hand, for the same VLT/X-shooter spectra, a decline in the total Na I D EW from 3.9 Å at +18.6 days to 3.3 Å at +27.1 days was reported. These measurements are discrepant from the ones reported here. This may be due to differences in the lens and host galaxy subtraction, or possibly a lack thereof in Johansson et al. (2021). Using our VLT/X-shooter spectra with neither lens nor host galaxy subtraction, we find comparable Na I D total EWs to Johansson et al. (2021) of 3.52 ± 0.18 Å and 3.13 ± 0.2 Å for the epochs +18.6 and +27.1 days, respectively. Hence, the EWs as measured by Johansson et al. (2021) represent lower limits. The time variability reported by Johansson et al. (2021) is possibly an effect of differences in the relative contribution of the lens and host galaxy flux in the two X-shooter spectra. These were observed at different position angles with the spectroscopic slit not covering the entire source. Indeed, time variability of Na I D EWs is not expected during the 8.5 day (rest-frame) period at the epochs of our X-shooter spectra (Blondin et al. 2009; Wang et al. 2019).

Our spectra have been corrected for lens galaxy contamination. To test for the possible effects of Na I D absorption contamination from the host galaxy we model the host galaxy using the elliptical galaxy template (Cano et al. 2018) that was also used to correct for lens galaxy contamination (Johansson et al. 2021; see the Appendix for a discussion of the spectral features of the lens and host galaxies). We subtract a scaled, linear combination of the lens and host spectral template at their respective redshifts and estimate the scaling factor from Figure 5 of Johansson et al. (2021). This shows that, at the position of the sodium complex, the host galaxy contributes about one-third of the total host+lens spectral energy flux. We then repeat the absorption line analysis described above on the lens+host-subtracted spectrum and obtain a total Na I D EW of 5.04 ± 0.25 Å (+18.6 days) and 4.8 ± 0.25 Å (+27.1 days), which is within the quoted uncertainties of our measurements (Tables 1 and 2). We note that the galaxy template has prominent Na I D absorption, which may overestimate the actual Na I D absorption from the host galaxy. Therefore, the effect can be considered as an upper limit and possible host galaxy contamination does not impact the results and conclusion of the paper.

4. The Origin of the Sodium Absorption Components

Large EWs, similar to those measured for SN 2016geu, have only been measured for four other SNe Ia in the nearby Universe: SN 1986G (D'Odorico et al. 1989), SN 2003cg (Blondin et al. 2009), SN 2006et (Wang et al. 2019), and SN 2014J (Ritchey et al. 2015). Hence, this poses the following question: why does this rare, lensed SN Ia belong to this select group of SNe Ia? To address this question we assess the origin of the resolved Na I D and Ca II H and K components, A, B, C1, and D.

4.1. Column Density Ratios and an Inhomogeneous Medium

Figure 3 and Table 1 show the EW ratios of individual components of the Na I and Ca II. The Na I D_2 to D_1 EW ratios are $EW(D_2)/EW(D_1) = 1.48 \pm 0.22$ (18.6 days) and 1.44 ± 0.23 (27.1 days), i.e., no variability. Values for the single components (A–D) are between 1.2 and 1.8. The Ca II EW(K)/EW(H) ratio is ∼1.7 at both epochs. For the homogeneous medium, EW ratios of 2 are expected for Na I D and Ca II from their respective oscillator strengths (*f*-values). Ratios closer to 1 imply an inhomogeneous medium: different subcomponents may only incompletely cover the continuum radiation source. Some such subcomponents may be saturated despite the fact that the observed absorption lines do not reach zero intensity

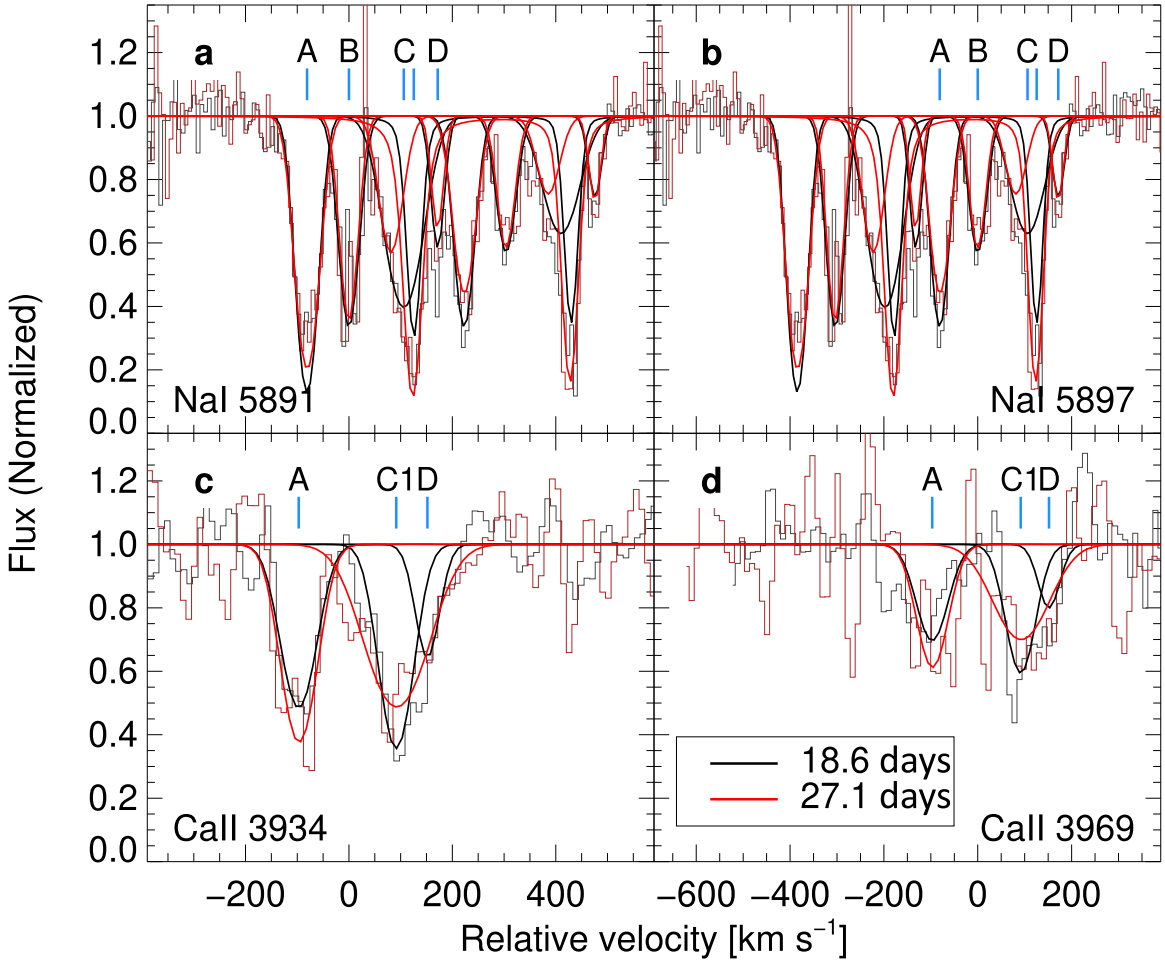

Figure 2. The sodium and calcium absorption line complex of SN 2016geu. The panels show (a), Na I D_2 λ5891, (b), Na I D_1 λ5897, (c), Ca II K λ3934, and (d), Ca II H λ3969. The black and red solid lines are the individual Voigt profile (Section 3) components from fits to the data at rest-frame epochs +18.6 and +27.1 days, respectively. There are five components labeled as A, B, C, and D, of which component C consists of two subcomponents C1 and C2 for each of the Na I D_1 and D_2 transitions, and three corresponding Ca II H and K components are labeled A, C1, and D. The horizontal dashed line indicates 1 in normalized flux units. All velocities are given relative to the redshift of component B, $z = 0.408788$.

(see Figures 1 and 2). A similar effect has been observed through quasar and galaxy sight lines across the Milky Way (Poznanski et al. 2012) and in other SNe Ia (D'Odorico et al. 1989; Stritzinger et al. 2010; Ritchey et al. 2015). Indeed, the Doppler broadening parameter, $b \gtrapprox 20$ km, for components A, B, and C1 implies the existence of multiple subcomponents unresolved in our data and, thus, supports the inference of an inhomogeneous medium.

To infer the nature of these subcomponents, we use the column density ratio, N(Ca II)/N(Na I). We obtain a ratio of 0.8 ± 0.1 for component A while C1 and D have ratios $\gtrsim 1$ (Figure 3). Similar ratios have been measured for, e.g., SN 1986G (D'Odorico et al. 1989) and SN 2014J (Ritchey et al. 2015). For component B the column density ratio, N(Ca II)/N(Na I), as well as the EW ratio, EW(Ca II)/EW (Na I), are both $\ll 1$. Measurements of column density ratios in interstellar sight lines show that N(Ca II)/N(Na I) $\gtrsim 1$ corresponds to warm, high-velocity (relative to the local standard of rest) clouds in which calcium is mostly liberated from dust grains. Conversely, ratios $\lesssim 1$ are typical of cold, dense molecular clouds in which large fractions of calcium are depleted onto dust grains (Siluk & Silk 1974; Vallerga et al. 1993). Consequently, the column density ratio of component A indicates moderate calcium depletion onto dust grains.

4.2. Component B

It is intriguing that there is no Ca II absorption at the position of component B. The strong calcium depletion of component B implies a molecular cloud origin.

The N(Ca II)/N(Na I) column density ratio is affected by variations in the ionization conditions of the absorbing material. Previous studies of SNe Ia with complex or time-varying Na I D have shown that due to the lower ionization potential and differences in the photoionization cross sections of Na I D compared to Ca II, Na I D is ionized out to radii $\approx 10^{19}$ cm, while Ca II may only be ionized out to shorter distances of less than 10^{18} cm (Patat et al. 2010; Ferretti et al. 2016). Other ionization calculations (Simon et al. 2009) show that at low distances to SNe Ia, first Na I D gets ionized and Ca II follows with some delay. However, Ca II may not be affected at all if the material is at a radius larger than $\approx 10^{17-18}$ cm. In such modeled ionization scenarios, the EW of Na I D_2 is predicted to be less than or equal to the EW of Ca II K (Simon et al. 2009) but can be larger if a significant fraction of calcium is depleted onto dust grains. This, together with the observed time invariability of the Na I D components, places component B at radii $\gtrsim 10^{17-18}$ cm away from the supernova, which is outside the supernova dust destruction

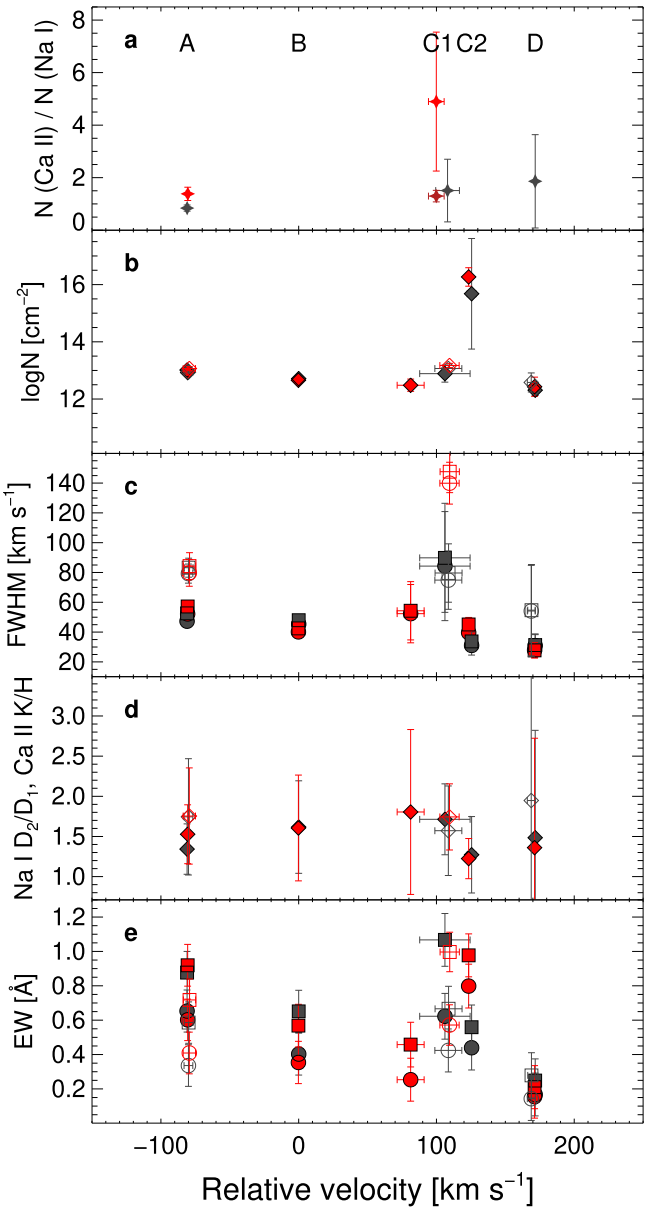

Figure 3. Parameters of the different Na I D and Ca II H and K components. Gray and red symbols are for epochs +18.6 and +27.1 days, respectively. Filled and open symbols are for Na I D and Ca II, respectively. Square symbols mark the Na I D_2 and Ca II K transitions, while circles mark the Na I D_1 and Ca II H transitions. All measurements are summarized in Tables 2 and 1. (a) The column density N(Ca II)/N(Na I D) ratio of components A, C1, and D. The dark red data point (+27.1 days) is the ratio N(Ca II(C1))/N(Na I D(C1+D)) at the velocity of component C1. (b) The column densities. (c) The full width at half-maximum (FWHM). (d) The equivalent width (EW) Na I D_2/D_1 and Ca II K/H ratios. (e) The EW values.

zone (Wang et al. 2019) and, hence, supports an interstellar origin. Furthermore, the redshift of the host galaxy (see Section 3) coincides with component B.

4.3. Components A, C, and D

The Na I D absorption component A is blueshifted by $\sim$80 km s^{-1}. In comparison, typical expansion velocities of circumstellar material are about 50 km s^{-1} (Patat et al. 2007; Dilday et al. 2012). Therefore, both higher-velocity blueshifted and redshifted Na I D or Ca II absorption components can have an origin in in- and outflowing material in the interstellar medium of galaxies. In this scenario a decline in dust depletion with velocity (Siluk & Silk 1974), as observed in SN 2016geu as well as in SN 1986G (D'Odorico et al. 1989) and SN 2014J (Ritchey et al. 2015), is expected. For SN 2016geu, this implies that the low, weighted-average host galaxy $E(B-V) = 0.22 \pm 0.04$ mag (Dhawan et al. 2020) is in fact dominated by the dusty interstellar absorbers (subcomponents) responsible for the Na I D components, i.e., A and B, while the higher-velocity Na I D components (i.e., C and D) contribute only marginally to the extinction. This scenario naturally explains why the Na I D EW of 5.2 Å measured for SN 2016geu is much larger than expected from existing empirical relations between dust extinction and Na I D EW in the Milky Way (Munari & Zwitter 1997; Poznanski et al. 2012).

5. Conclusion

In conclusion, the results demonstrate that not all Na I D-absorbing material must contain dust. Hence, $E(B-V)$ measured along the line of sight to SN 2016geu is not related to the total large Na I D EW of 5.2 Å. The observed characteristics (column density ratios, multiple components, and high EWs) of the Na I D and Ca II absorption systems of SN 2016geu (Figures 2 and 3) reflect a complex, interstellar, and circumgalactic in- and outflowing material. While the high-velocity blueshifted Na I D and Ca II component A could be due to outflowing circumstellar matter, there is no further evidence supporting such a scenario. However, there is hydrogen emission of the host galaxy of SN 2016geu (Johansson et al. 2021; see Appendix Figure 5) with a velocity dispersion that coincides with the velocity range of the Na I D. Consequently, such strong Na I D and Ca II absorption systems are likely linked to gas-rich star-forming regions, young stellar populations, or late-type host galaxies (Hopkins et al. 2012). Since there is evidence suggesting that the host galaxy is a massive galaxy dominated by an old stellar population, we conclude that the complex Na I D and Ca II originates from a star-forming region in a massive galaxy.

Acknowledgments

This investigation is based on observations made with ESO Telescopes at the La Silla Paranal Observatory under program ID 098.A-0648(A). This work is supported by a VILLUM FONDEN Young Investigator grant (project No. 25501). This work was supported by research grants (VIL16599, VIL54489) from VILLUM FONDEN. We thank Radek Wojtak and the anonymous referee for helpful comments and discussions.

Facility: VLT:Kueyen (XSHOOTER).

Software: Astropy (Astropy Collaboration et al. 2013, 2018), ESO / `ESOReflex` workflow versions 2.9.2 (Modigliani et al. 2010; Freudling et al. 2013), molecfit (Kausch et al. 2015; Smette et al. 2015), custom `python` programs[9] (Selsing et al. 2019), `VoigtFit` (Krogager 2018), custom IDL programs (Gall et al. 2024).

Appendix
Emission and Absorption Lines in the Host and Lens Galaxy

In this Appendix we provide an analysis of spectral features relating to the host and lens galaxies. These support our

[9] For program details see https://github.com/jselsing/xsh-postproc.

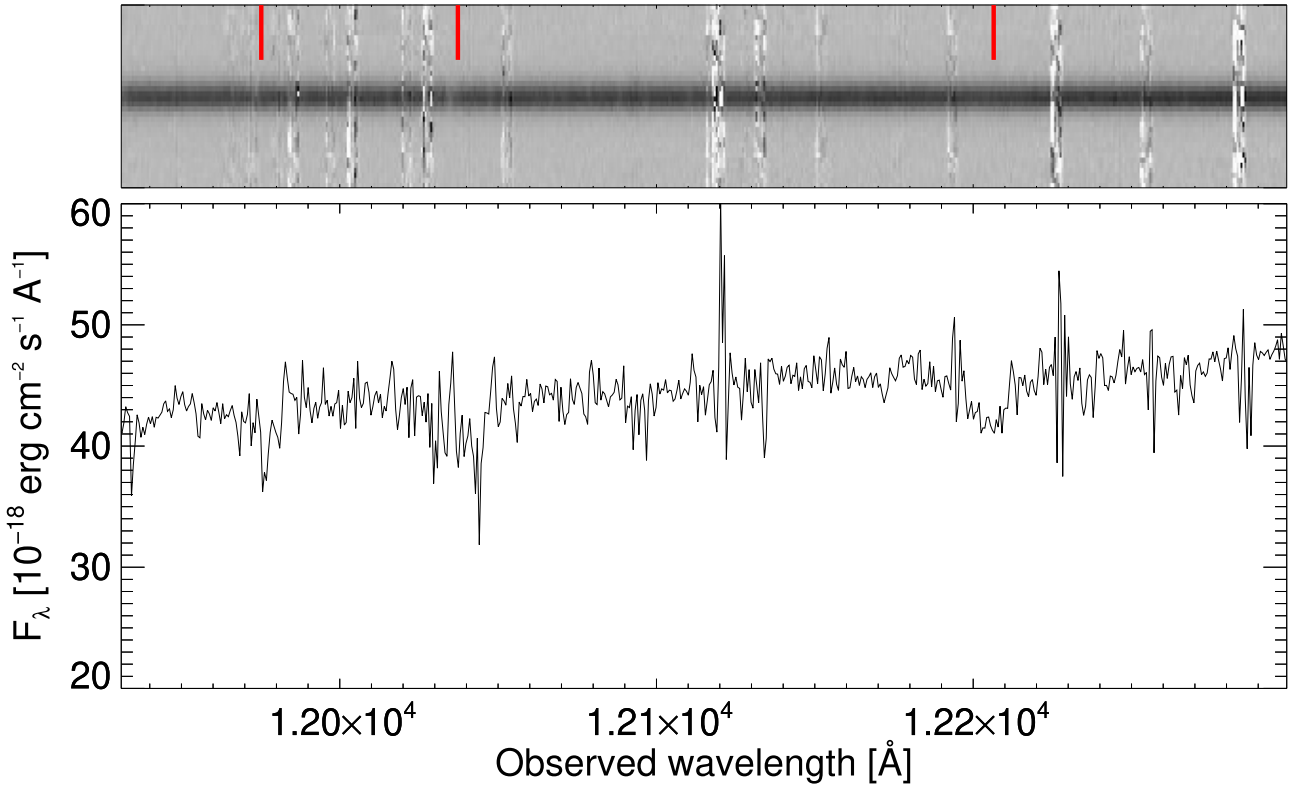

Figure 4. The Ca II near-infrared triplet in the host galaxy. Upper panel: the coadded VLT/X-shooter 2D spectrum of epochs +18.6 and +27.1 days. The expected Ca II triplet at $\lambda\lambda$ 8498, 8542, and λ8662 absorption lines are indicated as red solid lines at the redshift of the Na I D component B. Lower panel: the coadded VLT/X-shooter 1D spectrum of epochs +18.6 and +27.1 days.

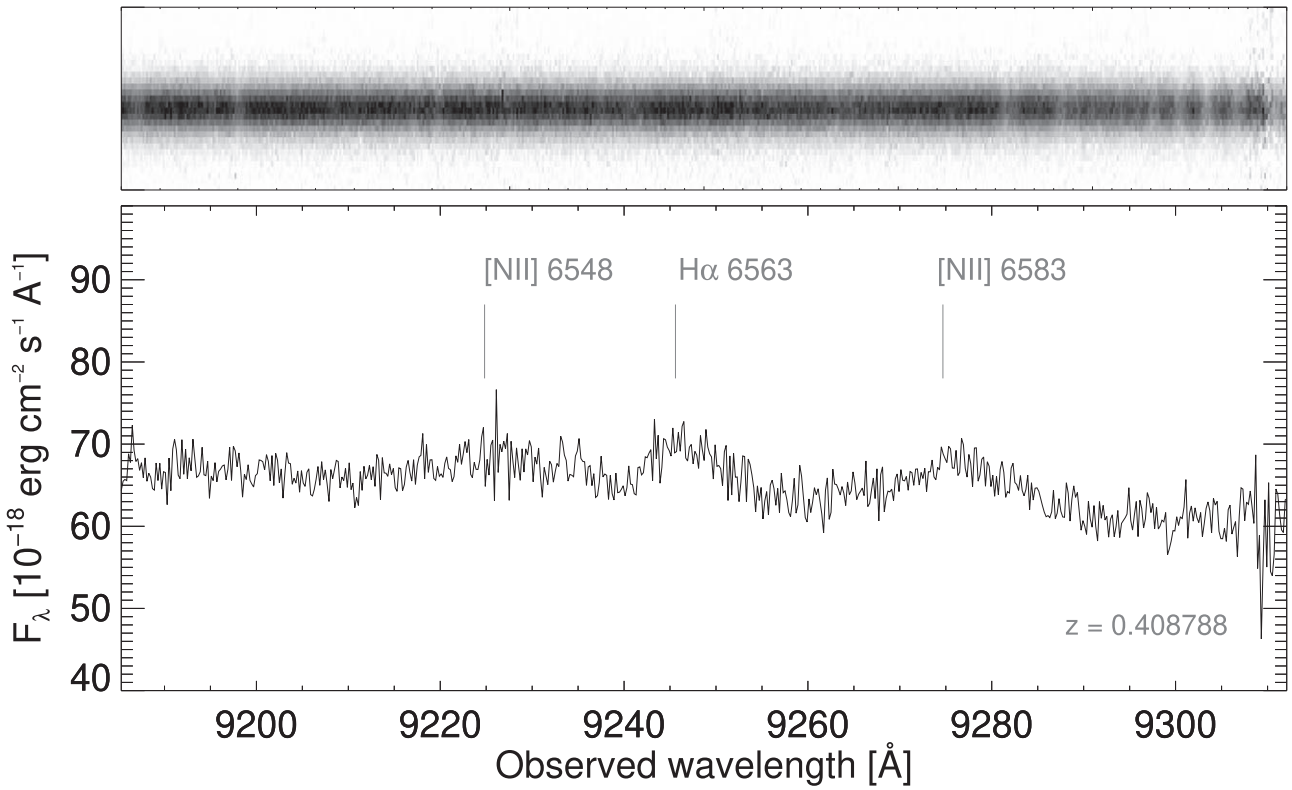

Figure 5. The Hα emission in the host galaxy. Upper panel: the coadded VLT/X-shooter 2D spectrum of epochs +18.6 and +27.1 days. Lower panel: the coadded VLT/X-shooter 1D spectrum of epochs +18.6 and +27.1 days. The gray annotations mark [N II] at $\lambda\lambda$ 6548.06 and 6583.45 Å and Hα emission at the redshift of the Na I D component B.

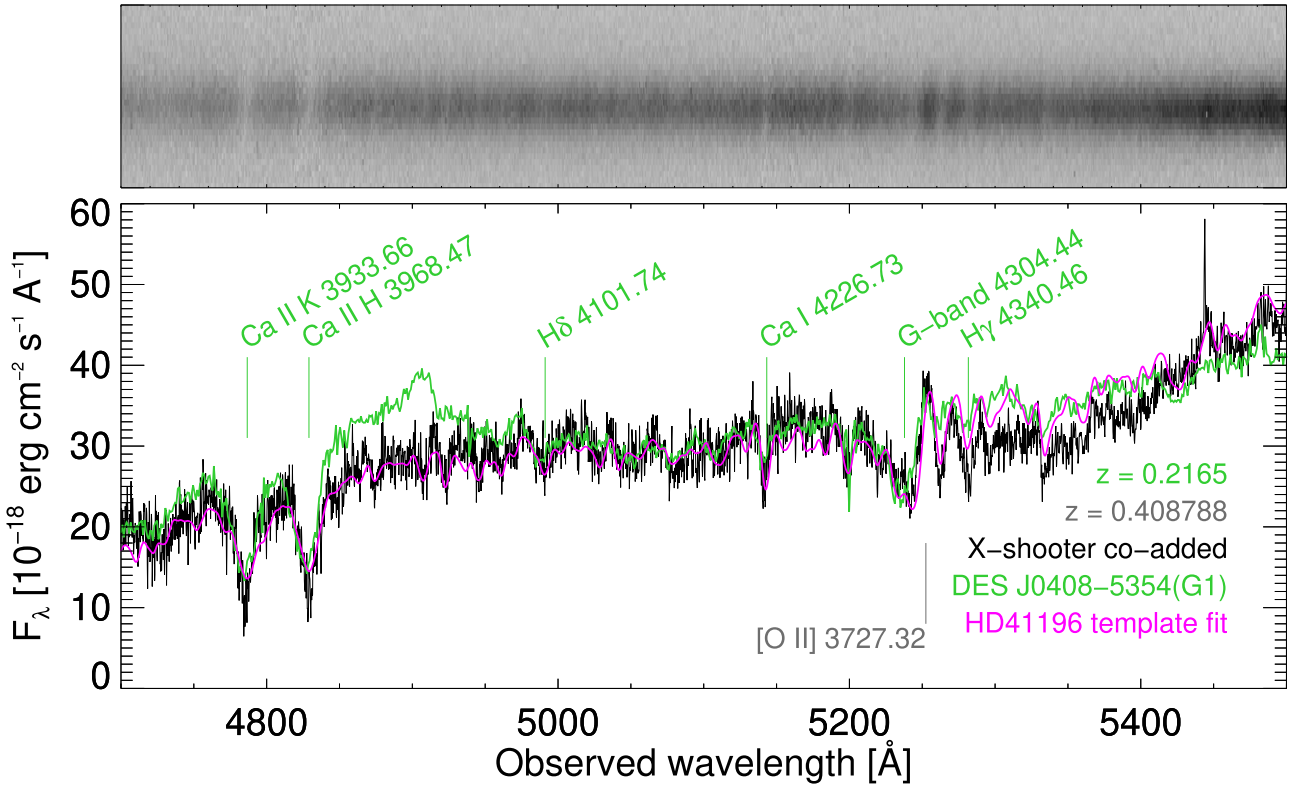

Figure 6. Disentangling lens and host galaxy. Upper panel: our coadded VLT/X-shooter 2D spectrum of epochs +18.6 and +27.1 days. Lower panel: our coadded VLT/X-shooter 1D spectrum of epochs +18.6 and +27.1 days (black). The green spectrum is the massive lens galaxy DES J0408-5354 G1 (Buckley-Geer et al. 2020) spectrum redshifted to match the redshift ($z = 0.2165$) of the lens galaxy of SN 2016geu and normalized in flux to match our coadded VLT/X-shooter spectrum. In magenta is the best-fit X-shooter spectrum of the star HD 41196 convolved to a velocity dispersion of 141 ± 5 km s^{-1} at the redshift of the lens galaxy ($z = 0.2164$). The gray annotation illustrates the position of [O II] at the redshift $z = 0.408788$ of the host galaxy of SN 2016geu as suggested by Johansson et al. (2021).

assumption of these galaxies being massive and dominated by old stellar populations.

Figure 4 shows weak absorption of the Ca II λ8662 line, the strongest line of the Ca II near-infrared triplet, which coincides with the redshift of the Na I D component B. We measure an FWHM of about 220 km s^{-1}. The Ca II line is observed at a wavelength of 12206.5 Å right in between two OH molecular skylines but is not affected by telluric absorption lines. The Ca II NIR triplet is a prominent feature observed in galaxies and originates in the photospheres of stars (Terlevich et al. 1990).

Figure 5 shows that there is weak [N II] λ6583 and Hα emission, as also noticed by Johansson et al. (2021), in the host galaxy with an FWHM $\sim$200 km s^{-1}, consistent with that of the Ca II λ8662 line. Both the lens and host galaxy Hα/[N II] flux ratios are $\sim$1, which is indicative of a massive galaxy and supersolar metallicity. However, we do not detect [O III] $\lambda\lambda$ 4959, 5007 Å, which is a typical signature for star-forming galaxies.

Figure 6 shows a conspicuous emission feature at an observed wavelength of λ5250, which has been suggested to be [O II] λ3727 (Johansson et al. 2021) at a redshift $z = 0.4087$ of the host galaxy. However, it is within a complex spectral region. To verify its nature, we coadded our two X-shooter spectra to increase the signal-to-noise ratio and compared this coadded spectrum to a similar massive lens galaxy spectrum. The conspicuous emission is consistent with spectral features typical of a massive galaxy, i.e., molecular CH absorption at $\sim\lambda$4304 (*G*-band) at a redshift of the lens galaxy $z = 0.2164$. Fitting our coadded X-shooter spectrum using the X-shooter spectrum of the star HD 41196 convolved with a velocity dispersion of 141 ± 5 km s^{-1} at the redshift of the lens galaxy can also explain the spectral features in the wavelength range 5200–5300 Å. Nevertheless, weak [O II] may be possible. Signatures of an old stellar population in the host galaxy include weak *G*-band or Mg I triplet absorption, also typical of a massive galaxy.

In some high-resolution spectra of SNe Ia that exhibit strong Na I D there is absorption from diffuse interstellar bands (DIBs) such as the DIB at λ5780 (Phillips et al. 2013; Graham et al. 2015). However, for SN 2016geu the DIB λ5780 is not detected (Johansson et al. 2021). Furthermore, we do not detect other DIBs at $\lambda\lambda$ 5797, 6196, 6203, 6270, 6284, 6379, 6614, and 6661 Å, molecular features such as CH^+ $\lambda\lambda$3957 and 4232 Å the CN violet band $\lambda \sim 3874$–3880 Å, or potassium K I $\lambda\lambda$7667 and 7701 Å absorption lines. These elements and molecules are less abundant than sodium or calcium, but some have been detected in sight lines toward SN 2014J and 1986G (D'Odorico et al. 1989; Welty et al. 2014; Ritchey et al. 2015). Assuming that the relation between interstellar Na and K column densities of N(Na II)/N(K I) $\approx$85 holds (Welty & Hobbs 2001), it is expected that we do not detect the K I $\lambda\lambda$ 7664,7698 Å doublet in our medium-resolution spectra. However, we estimate the 2σ upper limit for the EW of the DIB at λ5780 using the same method as Phillips et al. (2013) to be 0.24 Å. This, together with the extinction parameter $A_V = 0.58 \pm 0.09$ mag (Dhawan et al. 2020) places SN 2016geu within the 1σ dispersion region of the relation between the EW

of the 5780 Å DIB and the host galaxy extinction shown in Phillips et al. (2013, Figure 5).

ORCID iDs

Christa Gall https://orcid.org/0000-0002-8526-3963
Jens Hjorth https://orcid.org/0000-0002-4571-2306
Lise Christensen https://orcid.org/0000-0001-8415-7547
Luca Izzo https://orcid.org/0000-0001-9695-8472
Paolo A. Mazzali https://orcid.org/0000-0001-6876-8284
Mark M. Phillips https://orcid.org/0000-0003-2734-0796
Peter Hoeflich https://orcid.org/0000-0002-4338-6586
Charlotte Angus https://orcid.org/0000-0002-4269-7999
Cecilie Cold https://orcid.org/0000-0001-7666-1874
Jonatan Selsing https://orcid.org/0000-0001-9058-3892

References

Astropy Collaboration, Robitaille, T. P., Tollerud, E. J., et al. 2013, A&A, 558, A33
Astropy Collaboration, Price-Whelan, A. M., Sipőcz, B. M., et al. 2018, AJ, 156, 123
Benetti, S., Cappellaro, E., Mazzali, P. A., et al. 2005, ApJ, 623, 1011
Blondin, S., Prieto, J. L., Patat, F., et al. 2009, ApJ, 693, 207
Branch, D., Dang, L. C., Hall, N., et al. 2006, PASP, 118, 560
Buckley-Geer, E. J., Lin, H., Rusu, C. E., et al. 2020, MNRAS, 498, 3241
Cano, Z., Selsing, J., Hjorth, J., et al. 2018, MNRAS, 473, 4257
Clark, P., Maguire, K., Bulla, M., et al. 2021, MNRAS, 507, 4367
Dhawan, S., Johansson, J., Goobar, A., et al. 2020, MNRAS, 491, 2639
Dilday, B., Howell, D. A., Cenko, S. B., et al. 2012, Sci, 337, 942
D'Odorico, S., Dekker, H., Mazzoleni, R., et al. 2006, Proc. SPIE, 6269, 626933
D'Odorico, S., di Serego Alighieri, S., Pettini, M., et al. 1989, A&A, 215, 21
Ferretti, R., Amanullah, R., Goobar, A., et al. 2016, A&A, 592, A40
Foley, R. J., Simon, J. D., Burns, C. R., et al. 2012, ApJ, 752, 101
Freudling, W., Romaniello, M., Bramich, D. M., et al. 2013, A&A, 559, A96
Gall, C., Hjorth, J., Christensen, L., Izzo, L., Selsing, J., et al. 2024, Sodium towards SN 2016geu, Electronic Research Data Archive, Univ. of Copenhagen, doi:10.17894/UCPH.940A6E89-B8FF-4265-AF45-BFBE6AD06D0C
Goobar, A., Amanullah, R., Kulkarni, S. R., et al. 2017, Sci, 356, 291
Graham, M. L., Valenti, S., Fulton, B. J., et al. 2015, ApJ, 801, 136
Hillebrandt, W., & Niemeyer, J. C. 2000, ARA&A, 38, 191
Höflich, P., Kumar, P., & Wheeler, J. C. 2011, Cosmic Explosions in Three Dimensions (Cambridge: Cambridge Univ. Press)
Hopkins, P. F., Quataert, E., & Murray, N. 2012, MNRAS, 421, 3488
Horne, K. 1986, PASP, 98, 609
Hoyle, F., & Fowler, W. A. 1960, ApJ, 132, 565
Iben, I. J., & Tutukov, A. V. 1984, ApJS, 54, 335
Johansson, J., Goobar, A., Price, S. H., et al. 2021, MNRAS, 502, 510
Kausch, W., Noll, S., Smette, A., et al. 2015, A&A, 576, A78
Krogager, J.-K. 2018, arXiv:1803.01187
Livio, M., & Mazzali, P. 2018, PhR, 736, 1
Maguire, K., Sullivan, M., Patat, F., et al. 2013, MNRAS, 436, 222
Modigliani, A., Goldoni, P., Royer, F., et al. 2010, Proc. SPIE, 7737, 773728
More, A., Suyu, S. H., Oguri, M., More, S., & Lee, C.-H. 2017, ApJL, 835, L25
Morton, D. C. 1991, ApJS, 77, 119
Munari, U., & Zwitter, T. 1997, A&A, 318, 269
Nomoto, K. 1982, ApJ, 253, 798
Patat, F., Chandra, P., Chevalier, R., et al. 2007, Sci, 317, 924
Patat, F., Chugai, N. N., Podsiadlowski, P., et al. 2011, A&A, 530, A63
Patat, F., Cox, N. L. J., Parrent, J., & Branch, D. 2010, A&A, 514, A78
Phillips, M. M., Simon, J. D., Morrell, N., et al. 2013, ApJ, 779, 38
Poznanski, D., Prochaska, J. X., & Bloom, J. S. 2012, MNRAS, 426, 1465
Raskin, C., & Kasen, D. 2013, ApJ, 772, 1
Ritchey, A. M., Welty, D. E., Dahlstrom, J. A., & York, D. G. 2015, ApJ, 799, 197
Schlafly, E. F., & Finkbeiner, D. P. 2011, ApJ, 737, 103
Selsing, J., Malesani, D., Goldoni, P., et al. 2019, A&A, 623, A92
Siluk, R. S., & Silk, J. 1974, ApJ, 192, 51
Simon, J. D., Gal-Yam, A., Gnat, O., et al. 2009, ApJ, 702, 1157
Smette, A., Sana, H., Noll, S., et al. 2015, A&A, 576, A77
Soker, N., Kashi, A., García-Berro, E., Torres, S., & Camacho, J. 2013, MNRAS, 431, 1541
Sternberg, A., Gal-Yam, A., Simon, J. D., et al. 2011, Sci, 333, 856
Stritzinger, M., Burns, C. R., Phillips, M. M., et al. 2010, AJ, 140, 2036
Terlevich, E., Díaz, A. I., & Terlevich, R. 1990, RMxAA, 21, 218
Vallerga, J. V., Vedder, P. W., Craig, N., & Welsh, B. Y. 1993, ApJ, 411, 729
Vernet, J., Dekker, H., D'Odorico, S., et al. 2011, A&A, 536, A105
Wang, X., Chen, J., Wang, L., et al. 2019, ApJ, 882, 120
Webbink, R. F. 1984, ApJ, 277, 355
Welty, D. E., & Hobbs, L. M. 2001, ApJS, 133, 345
Welty, D. E., Hobbs, L. M., & Kulkarni, V. P. 1994, ApJ, 436, 152
Welty, D. E., Ritchey, A. M., Dahlstrom, J. A., & York, D. G. 2014, ApJ, 792, 106
Whelan, J., & Iben, I. J. 1973, ApJ, 186, 1007